

Structural Insights into *Schistosoma mansoni* Carbonic Anhydrase (SmCA) Inhibition by Selenoureido-Substituted Benzenesulfonamides

Andrea Angeli,* Marta Ferraroni,* Akram A. Da'dara, Silvia Selleri, Mariana Pinteala, Fabrizio Carta, Patrick J. Skelly, and Claudiu T. Supuran



Cite This: *J. Med. Chem.* 2021, 64, 10418–10428



Read Online

ACCESS |



Metrics & More

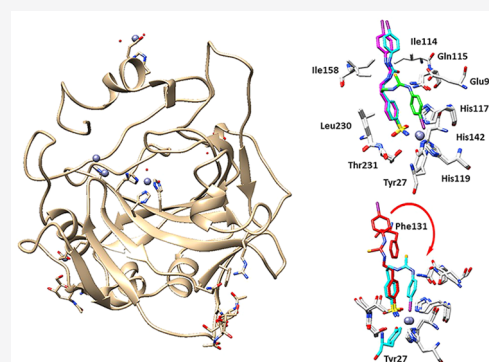


Article Recommendations



Supporting Information

ABSTRACT: Tegumental carbonic anhydrase from the worm *Schistosoma mansoni* (SmCA) is considered a new anti-parasitic target because suppressing its expression interferes with schistosome metabolism and virulence. Here, we present the inhibition profiles of selenoureido compounds on recombinant SmCA and resolution of the first X-ray crystal structures of SmCA in adduct with a selection of such inhibitors. The key molecular features of such compounds in adduct with SmCA were obtained and compared to the human isoform hCA II, in order to understand the main structural factors responsible for enzymatic affinity and selectivity. Compounds that more specifically inhibited the schistosome versus human enzymes were identified. The results expand current knowledge in the field and pave the way for the development of more potent antiparasitic agents in the near future.



INTRODUCTION

Schistosomiasis is classified as a neglected tropical disease caused by parasitic flatworms called blood flukes.¹ Currently, the WHO considers schistosomiasis among the principal neglected tropical diseases afflicting subtropical and tropical regions. Metadata analyses estimated that about 779 million people on the planet are exposed to risk of infection^{2,3} and over 250 million are infected with *Schistosoma* spp., of which up to 201.5 million are in Africa.^{2–4} The six schistosome species able to infect humans have different geographical distributions and complex life cycles. *Schistosoma haematobium* and *S. mansoni* are endemic in sub-Saharan Africa and South America. Although *S. japonicum* is endemic in Asia, extensive measures of control and intervention allowed its complete eradication in the late 1970s in Japan.⁵ *S. mekongi*, *S. intercalatum*, and *S. guineensis* have substantially lower global prevalence. Schistosomiasis when untreated may result in considerable morbidity (*i.e.*, when caused by *S. mansoni* and *S. japonicum*, the infection is usually characterized by high parasite egg burdens) and even mortality.^{6,7} Despite intensive efforts, there is no vaccine currently available to prevent schistosome infections.^{8,9} The disease control is essentially limited to treatment with the most effective and widely used compound praziquantel (PZQ), an acylated quinoline–pyrazine compound which still is the pharmacological mainstay of schistosomiasis treatment for almost three decades.¹⁰ Reports of the failure of PZQ to cure infected patients in different geographic locations,^{11,12} as well as the experimental

selection of parasites refractory to PZQ treatment,¹³ are suggestive of the occurrence of drug resistance. These findings sustain the need to pursue research efforts toward generation of new anti-schistosome compounds. Recent advances in proteomic studies made it possible to identify new rational drug targets.^{14,15} Among these, an α -Carbonic Anhydrase (CA, EC 4.2.1.1) has been identified in *S. mansoni* worms and designated as SmCA. This is a 323-amino acid, GPI-linked protein that is expressed at the host-interactive surface of intravascular life stages and that has been shown to be essential for the worms to establish infection.^{14,16,17} SmCA has all features of α -CA protein family members, including conserved catalytic residues and metal binding sites.

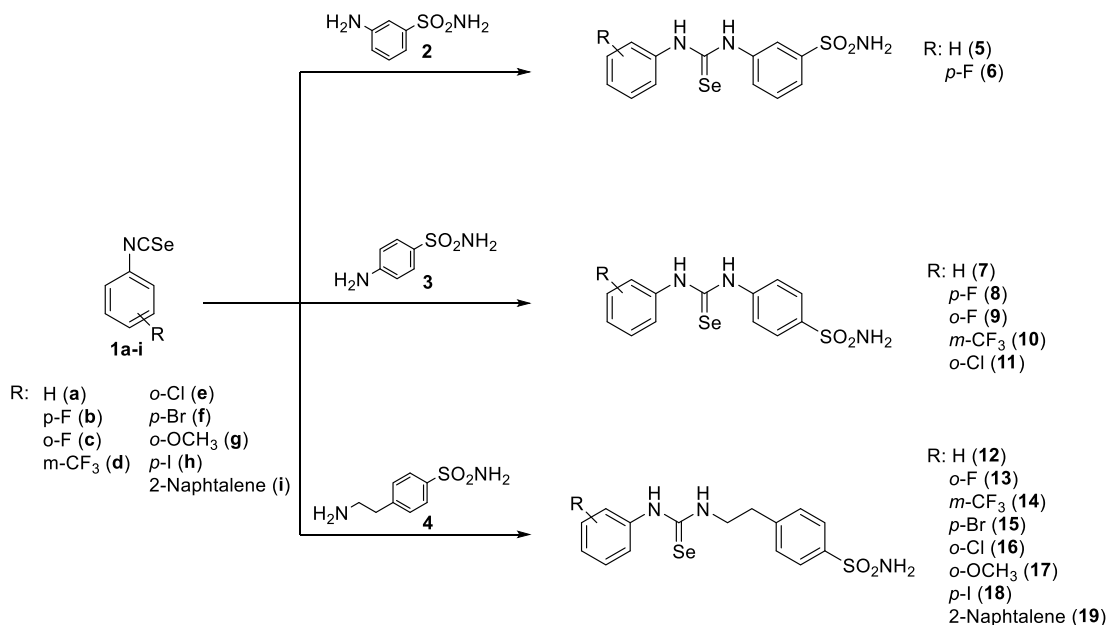
CAs are ubiquitous metalloenzymes able to reversibly catalyze the hydration of CO₂ to H⁺ and HCO₃[−].¹⁸ The purified recombinant SmCA possesses extremely rapid CO₂-hydration kinetics too.¹⁶ CA enzymes participate in a wide range of physiologic reactions including respiration, photosynthesis, pH regulation, electrolyte secretion, and many biosynthetic reactions.^{19–21} In recent years, much effort has been made to develop new CA inhibitors as novel therapeutics

Received: May 9, 2021

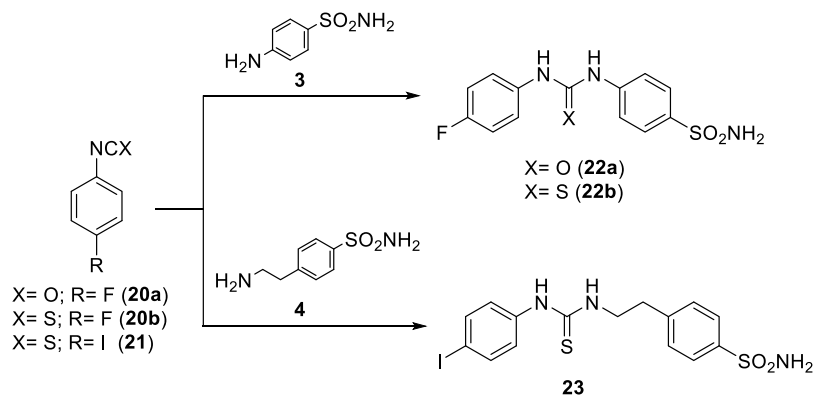
Published: July 7, 2021



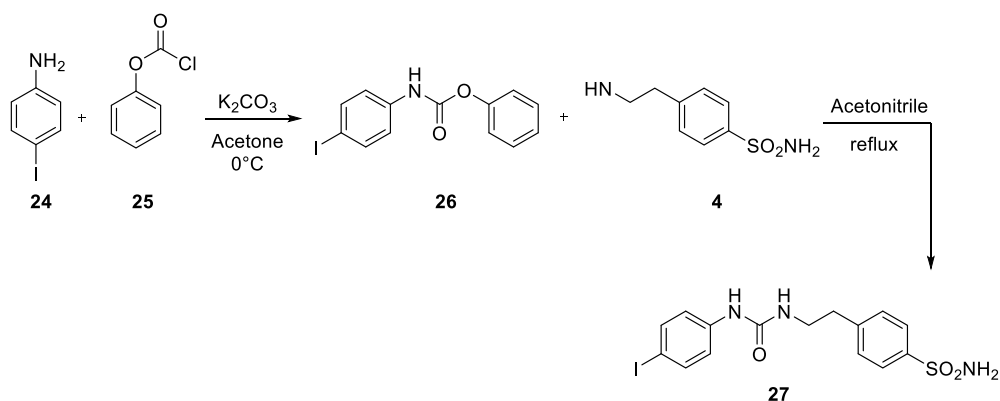
Scheme 1. General Synthesis of Selenoureido Derivatives 5–19



Scheme 2. General Procedure for the Synthesis of Ureido and Thio Ureido Derivatives 22a–b and 23



Scheme 3. General Procedure for the Synthesis of Ureido Derivative 27



to treat neglected tropical diseases and to mitigate the impact of drug resistance that is arising in common anti-parasitic drugs clinically in use.^{22–25} It is imperative to identify the structural differences between human CAs and parasite CAs in order to develop potent and selective inhibitors as novel anti-infective drugs. Because large differences between the crystal structure of SmCA and the physiologically dominant human isoform

hCA II have previously been shown in terms of regional conformation, active-site configuration, and in the length of connections between strands,¹⁶ it is worth speculating that selective SmCA inhibitors can be identified and developed.

To date, various classes of CA inhibitors have been developed and are currently used in clinics for the treatment of diseases.^{18,26,27} The ureido-substituted benzenesulfonamides

were reported to selectively inhibit hCA IX over the remaining human isoforms,²⁸ and one of these (*i.e.*, SLC-0111) is under Phase 2 clinical trial evaluation in association with gemcitabine for the treatment of solid pancreatic cancers. Here, we report the synthesis of a series of a selenoureido compounds, their *in vitro*-inhibition profiles against SmCA, and X-ray structural characterization of SmCA complexed with a selection of such compounds to decipher the structural factors contributing to the selective inhibition of such an enzyme. The results here reported will be useful in the near future to generate potent, specific SmCA inhibitors as lead compounds for the development of new drugs to impede vital schistosome metabolism and cure schistosome infection.

RESULTS AND DISCUSSION

Different aromatic isoselenocyanates **1a–h** were used to prepare the corresponding selenoureido derivatives **5–19** by standard coupling reactions with commercially available benzenesulfonamides **2–4** (Scheme 1), as reported earlier by our group.²⁹

With a similar procedure, the synthesis of ureido and thioureido derivatives **22a–b** and **23** is accomplished, using the corresponding thio or isocyanate (**20a–b** and **21**) as outlined below in Scheme 2.

In order to explore the other possible synthetic pathway to obtain ureido derivatives, we used 4-iodoaniline (**24**) and phenyl chloroformate (**25**) to obtain the corresponding carbamate **26** in excellent yield. Subsequently, the ureido benzenesulfonamide **27** is obtained by direct aminolysis of the aryl *N*-phenylcarbamates **26** with sulfonamide **4** as reported in Scheme 3.

Carbonic Anhydrase Inhibition. All compounds **5–19**, **22a–b**, **23**, and **27** were tested *in vitro* for their inhibitory activity against the recombinant CA from *S. mansoni* (SmCA) and the human off-target CA isoforms I and II by means of stopped-flow carbon dioxide-hydration assay.³⁰ Their activities were compared to the standard CA inhibitor acetazolamide (AAZ) and summarized in Table 1. The selectivity ratios for inhibition of SmCA over the ubiquitously expressed hCA II is also presented.

The aim of the study was to observe how the selenoureido compounds (**5–19**) and their isosters (**22a–b**, **23**, and **27**) influenced the potency and selectivity against SmCA. Compounds **5** and **6**, with a sulfonamide group at *meta* position, showed weak inhibition against hCAs and compound **5** also against SmCA. On the other hand, compound **6** with a fluorine atom at *meta* position showed good selectivity against SmCA with a ratio of 4.2. From the general point of view, the potency of selenoureido derivatives, against the SmCA, is increased when the sulfonamide group is placed at *para* position (**7–19**), leading to a low nanomolar inhibition constant. In particular, the potency of compounds **7–11** was observed to be highly influenced by the different substituents on the scaffold. Indeed, compound **7**, without a substituent, showed a lower inhibition potency among them (K_i 83.7 nM). On the other hand, compound **10** with a CF₃ substituent at *meta* position showed good selectivity against SmCA with a selectivity ratio of 4.1. The addition of an ethyl linker between the selenoureido scaffold and benzenesulfonamide in compounds **12–19** did not increase significantly the potency of inhibition but affected the selectivity. The *meta* substitution proved to be a key feature for selenoureido derivatives without the linker (**6**), increasing the selectivity against SmCA. With

Table 1. Inhibition Data of Human CA Isoforms I and II and SmCA with Compounds 5–19, 22a–b, 23, 27, and AAZ by Stopped-Flow CO₂-Hydration Assay³⁰

Cmp	K_i (nM) ^b			
	hCA I ^a	hCA II ^a	SmCA	ratio selectivity hCA II/SmCA
5	483.8	343.2	426.0	0.8
6	435.3	388.9	91.4	4.2
7	132.5	54.3	83.7	0.6
8	152.3	66.3	76.8	0.9
9	5.9	6.3	5.7	1.1
10	32.7	6.1	1.5	4.1
11	7.9	4.0	6.8	0.6
12	6.7	5.5	3.2	1.7
13	44.1	7.9	7.9	1
14	8.5	4.4	4.5	0.97
15	51.7	1.8	1.7	1.05
16	8.3	3.5	5.8	0.6
17	6.0	4.5	6.1	0.7
18	267.4	57.6	4.7	12.2
19	501.7	91.2	84.9	1.1
22a	5080	96.0	54.3	1.7
22b	35.0	14.2	23.3	0.6
23	74.1	7.6	37.6	0.2
27	80.1	7.8	13.3	0.6
AAZ	250.0	12.8	42.5	0.3

^aReferences 29 and 31. ^bMean from three different assays by a stopped-flow technique (errors were in the range of ± 5 to 10% of the reported values).

the addition of the linker (**12–19**), the compounds with a substituent at *para* position showed higher selectivity as in compound **18** which has an iodine atom (hCA II/SmCA = 12.2). In order to study how the isosteric replacement of selenium with sulfur and oxygen (**22a–b**, **23**, and **27**) could influence the potency and selectivity against SmCA, the isosters of compound **8** (**22a–b**) and the most selective **18** (**23** and **27**) were further investigated. The replacement of selenium with sulfur (**22b**) increased the potency of inhibition against SmCA (K_i 76.8 to 23.3 nM), whereas the selectivity decreased (hCA II/SmCA 0.9 to 0.6). On the other hand, the replacement with oxygen (**22a**) resulted in higher potency (K_i 54.3 nM) and a better selectivity ratio (hCA II/SmCA 1.7). A different behaviour is shown by isosters of derivative **18**. Both replacement with sulfur (**23**) or oxygen (**27**) decreased drastically the selectivity ratio against SmCA to 0.6 and 0.2, respectively, keeping high the potency of inhibition.

X-ray Study. In order to explain the inhibitory differences against hCA II and SmCA in terms of structural changes, a selection of the ureido compounds in complex with SmCA and hCA II were studied by X-ray crystallography. The first compound selected was derivative **8** (and its isosters **22a–b**) due to the well-known interaction with human CA isoforms.³² The second seleno derivative chosen was compound **18** (and its isosters **23** and **27**) due to the high potency and selectivity against SmCA.

Recombinant SmCA, previously crystallized by our group in the P3₂21 space group,¹⁶ is a glycosylated enzyme, which shared with all other α -CAs the same tertiary fold, with a central ten-stranded twisted beta-sheet as the dominant secondary structure element. In the search for optimal crystallization conditions, we found one that involves the use of 20% w/v PEG 3000, 0.2 M zinc acetate dihydrate, and 0.1

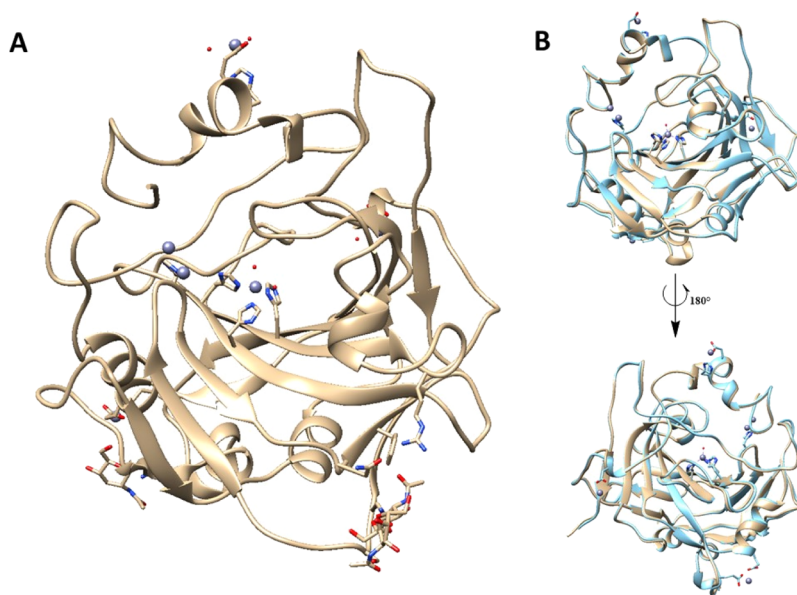


Figure 1. (A) X-ray crystal structures of SmCA in the tetragonal space group $P4_12_12$ (PDB accession code: 7O2S). (B) Comparison of tetragonal SmCA with the previously determined SmCA structure (PDB accession code: 6QQM). The tetragonal SmCA is in brown and trigonal SmCA in cyan; the gray sphere represents the zinc atom in the active site.

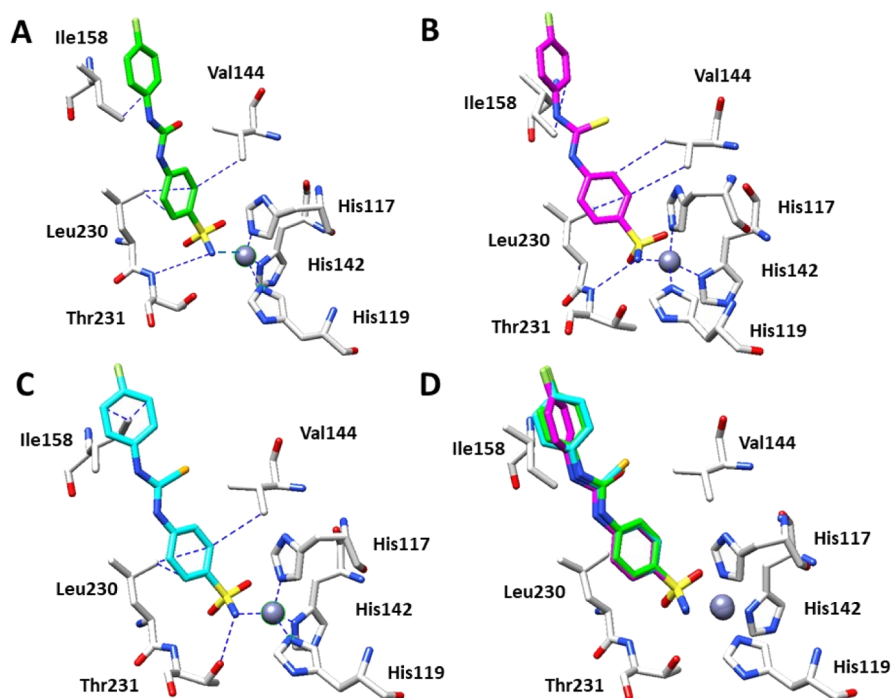


Figure 2. X-ray crystal structures of SmCA bound with compound 22a [(A) PDB: 7NWY], 22b [(B) PDB: 7NEX], and 8 [(C) PDB: 7BM4]. Panel (D) shows their superimposition in the active site. Residues involved in the binding of inhibitors are also shown; the gray sphere represents the zinc atom in the active site of the proteins.

M Imidazole (pH 8.0). The crystals grown from this solution belong to the tetragonal space group ($P4_12_12$), with one molecule per asymmetric unit. The X-ray crystal structure of this new form of SmCA (Figure 1A) was solved to investigate potential differences with the previously reported trigonal crystal structure of the protein.¹⁶

From the superposition of the two models, we found no substantial changes occurring between the two structures of SmCA (Figure 1B). The major difference is the presence of several zinc ions bound to residues His38, His88, Asp58, and

Glu175 in the tetragonal form. This new crystallization condition requires a different pH compared with previous crystallization conditions (pH 8.0 instead of pH 5.0) and could be useful for the preparation of complexes of compounds with pH sensitivity. However, because the selenoureido derivatives are not pH sensitive and the data obtained from crystals of the new form possess a lower resolution limit, we chose to use the trigonal crystals for the present study.

As regards the first inhibitors (compound 8 and its isomers 22a and 22b), after the initial rounds of refinement, the $F_o -$

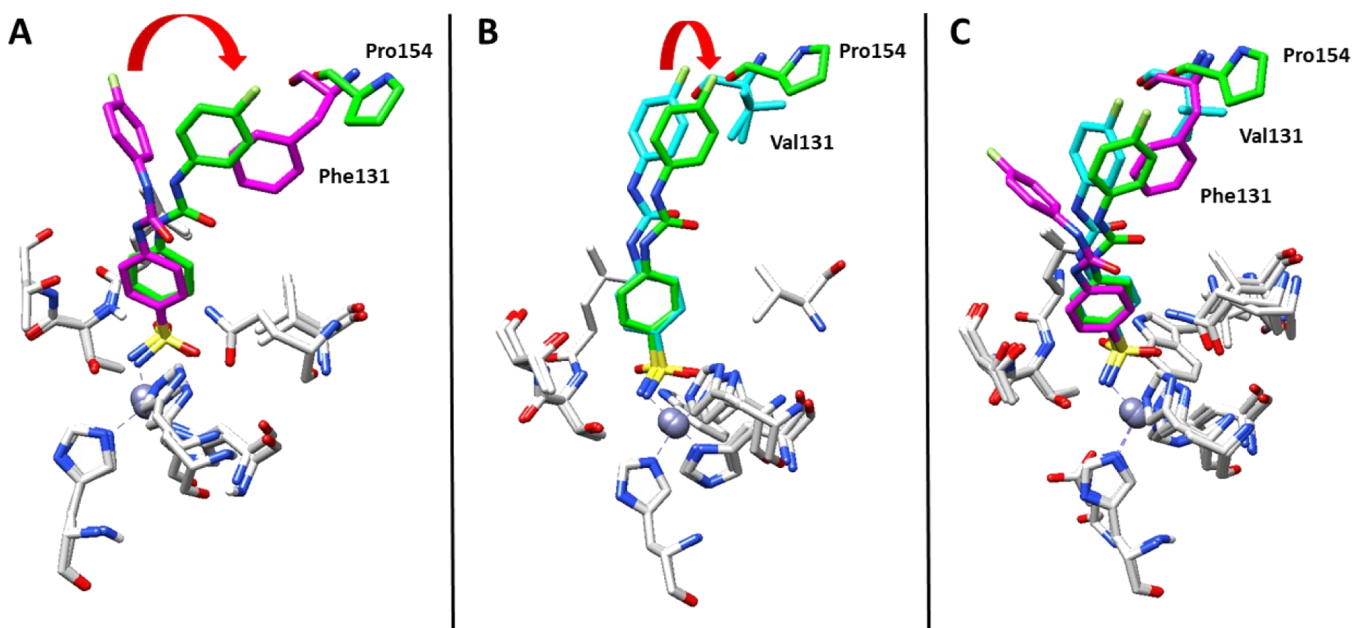


Figure 3. Overlay of compound 22a with hCA II, hCA IX mimic, and SmCA: (A) 22a hCA II (magenta)/22a SmCA (green), (B) 22a hCA IX mimic (cyan)/22a SmCA (green), and (C) overlay of compound 22a with all three isoforms. Specific residues are labeled.

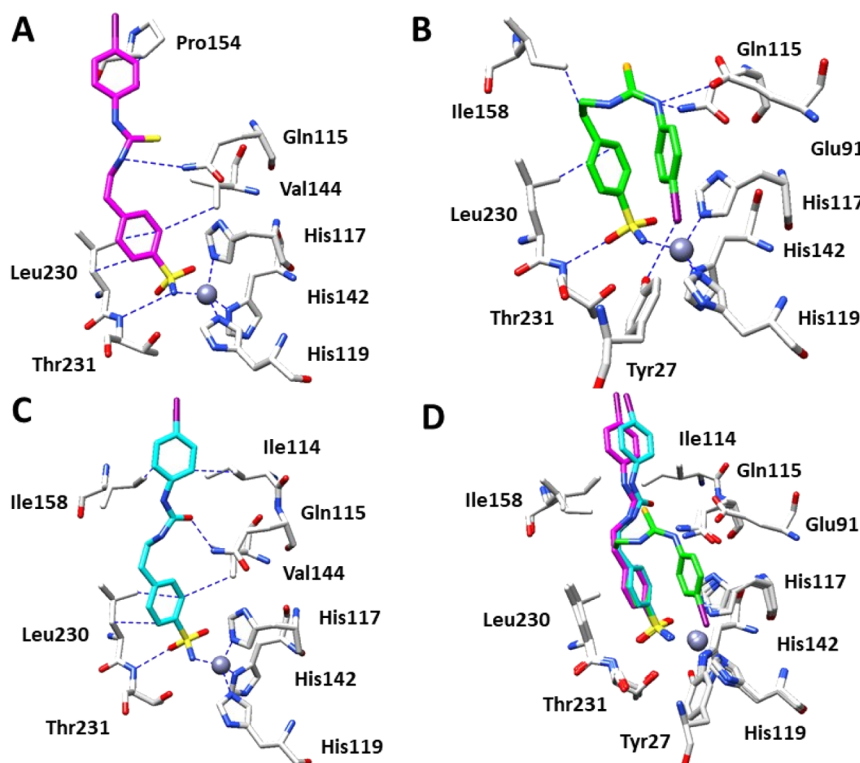


Figure 4. X-ray crystal structures of SmCA bound with compound 23 [(A) PDB: 7O48], 18 [(B) PDB: 7NG1], and 27 [(C) PDB: 7OAI]. Panel (D) showed their overlays in the active site. Residues involved in the binding of inhibitors are also shown and the gray sphere represents the zinc atom in the active site of the proteins.

Fc map showed a clear density for the compounds, in particular for the sulfonamide moiety which interacts directly with the zinc atom in the active sites (Figure S1). In all the three complexes, the sulfonamide moiety forms a hydrogen bond with the active site residue Thr231 in a similar manner as in the complexes with hCA II (Figure 2).

However, in all three complexes, the zinc ions and the inhibitors were introduced in the model with partial

occupancy, around 0.70. Additionally, we found that in the complexes with 22a and 22b, the side chain of one of the zinc ligands, His117, is in double conformation and at one position is not at a coordination distance with the zinc ion. All three compounds (8, 22a, and 22b) showed similar interactions inside the active site, forming hydrophobic connections between Leu230, Val144, and the benzenesulfonamide moiety and between Ile158 and the aromatic ring bearing the fluorine

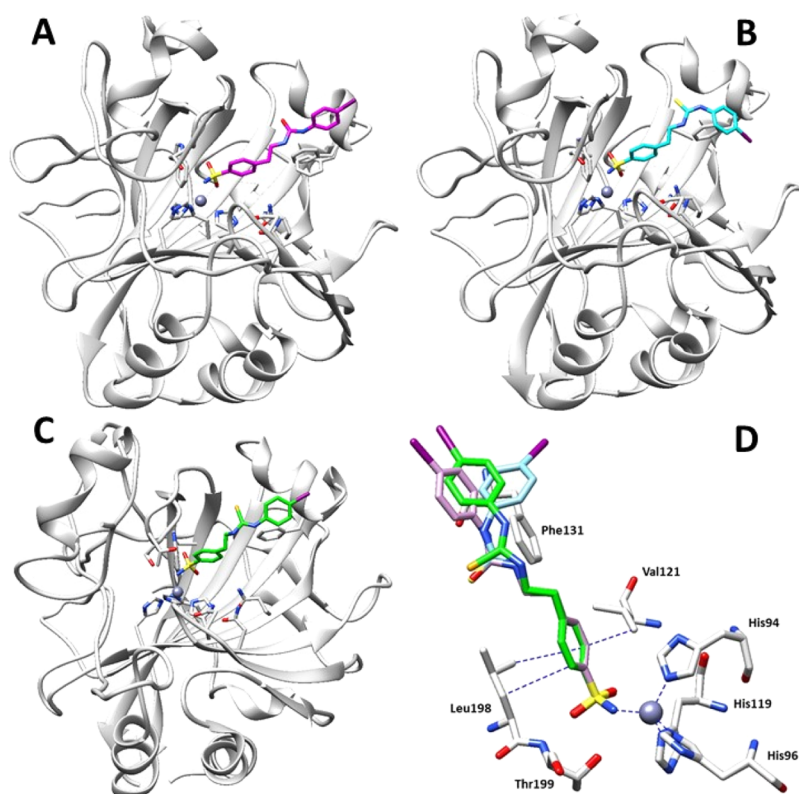


Figure 5. X-ray crystal structures of hCA II bound with compound 27 [(A) PDB: 7BG5], 23 [(B) PDB: 7BFA], and 18 [(C) PDB: 7BHH]. Panel (D) shows their overlays in the active site. Residues involved in the binding of inhibitors are also shown, and the gray sphere represents the zinc atom in the active site of the proteins.

atom. A superimposition of the three complexes (Figure 2D) did not show significant differences except for the aromatic ring with the fluorine atom which is slightly rotated in compounds 8 and 22b with respect to 22a due to different interactions with residue Ile158. These differences however do not influence significantly the location of the inhibitors inside the active site, reflecting the same-range potency of inhibition (K_i 23.3 to 76.8 nM). In compound 22a, the oxygen of the ureido moiety and the corresponding sulphur and selenium atoms in compounds 22b and 8 form a strong hydrogen bond with the side chain of residue Gln115, which also assumes two different conformations in compounds 22a and 22b.

Deep crystallographic studies of compound 22a have already been accomplished on different human CA isoforms such as II and IX^{31,33} and a direct comparison with SmCA is outlined in Figure 3.

The structural comparison showed similar features such as the benzene sulfonamide interactions with the catalytic zinc atom and with Thr 200/231 (hCA II/IX and SmCA, respectively). On the other hand, the inhibitor tail conformation shows substantial differences. In hCA II, Phe131 contributes to this conformational change, reducing the opening of the active site and acting as a binding anchor for the inhibitor tails (Figure 3A). In hCA IX, the corresponding residue is Val131, a less bulky residue, which makes the active site opening more accessible (Figure 3B). In SmCA, this residue is replaced by Pro154 which makes this part of the catalytic cavity more similar to that of the hCA IX mimic. Superposition of the three isoforms in complex with compound 22a (Figure 3C) clearly shows that the conformation of the inhibitor changes when this position is

replaced with a less bulky side chain such as proline (SmCA) with a tail rotation of 55°. In parallel, we noticed an increased affinity of the compounds for these isoforms.³¹ In addition, as previously reported, the crystal structures of 8 and 22b in complex with hCA II showed almost identical allocations within the enzyme cavity compared to 22a.²⁹

We found even more interesting structural features on moving to the second series of inhibitors (18, 23, and 27) complexed with SmCA. A clear electron density map of these compounds was observed inside the active site of the protein (Figure S1). The benzenesulfonamide scaffold showed the typical binding mode as mentioned above. In compounds 27 and 23b, the interactions with Leu230 and Val144 block the aromatic tails in a hydrophobic pocket, as already observed for the first series of inhibitors.

On the other hand, the electron density of the aromatic ring bearing the iodine substituent was scarce in the difference maps, owing probably to the fact that it is located at the rim of the active site and shows great mobility and disorder, and this part of the two inhibitors was omitted from the refinement.

Unexpectedly, the replacement of the ureido or thioureido group with selenoureido in compound 18 substantially changed the location of the tail inside the active site of SmCA (Figure 4B). Indeed, the bigger selenium atom moves the selenoureido moiety of compound 18 to a different conformation stabilized by two hydrogen bonds with Gln115 and Glu91 and by a hydrophobic interaction between Ile158 and the ethyl linker of the benzenesulfonamide. These particular interactions moved the tail of 18 (Figure 4D) to a different pocket, more hydrophilic (Figure S3), allowing the formation of a halogen bond between the iodine atom and the

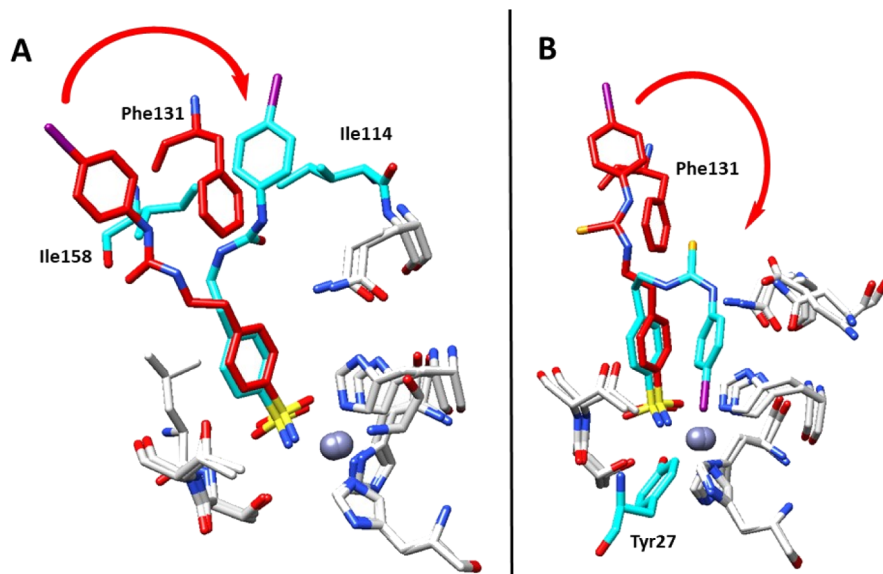


Figure 6. Overlay of compound 27 and 18 with hCA II and SmCA: (A) 27 hCA II (red)/27 SmCA (cyan) and (B) 18 hCA II (red)/18 SmCA (cyan). Specific residues are labeled.

hydroxyl group of the Tyr27 side chain (distance 3.3 Å), explaining the selectivity of this inhibitor against SmCA. In fact, in hCA II, compounds 18, 23, and 27 had similar binding modes as outlined in Figure 5. Phe131 plays a key role in these complexes, constraining the compounds to have the same orientation up to the ureido moiety. In correspondence of the *para*-iodophenyl moiety, the electron density was weak as already observed for the SmCA complexes with compounds 23 and 27 (Figure S2).

A structural comparison of ureido compound 27 with hCA II and SmCA showed a different location of the tail with a rotation of 60°. Anyway, compound 27 sits in a similar hydrophobic pocket of the active site created by the binding anchor Phe131 in hCA II or sandwiched between the two residues Ile114 and Ile158 in SmCA (Figure 6A). These features explain the similar potency and the absence of selectivity between the two CAs. On the other hand, the bulky selenoureido moiety and the absence of a binding anchor such as Phe131 in hCA II allowed compound 18 to change its tail conformation by rotating it by 150°. This rotation permits the formation of a specific halogen bond between the iodine atom and the hydroxyl of Tyr27 (Figure 6B).

These observations, taken together, explain the increase in interactions for compound 18 bound to SmCA compared to hCA II and therefore the 12.2-fold selectivity of binding for SmCA over hCA II.

In Vivo Efficacy. In order to test the effects of SmCA inhibitors on schistosomes *in vivo*, mice were first infected percutaneously with larval parasites (cercariae). Next, some mice were treated three times with selected compounds (7, 16, or 22a), each at its maximum tolerable dose. Control mice were treated with carrier dimethyl sulfoxide (DMSO) alone. Two weeks after the final treatment, worms were recovered from all mice and counted. These worm-burden data are presented in Figure 7. Each data point represents the number of worms from an individual mouse and the lines represent the mean for each group.

There was no significant difference in mean worm numbers recovered from any treated group *versus* control ($p = 0.1161$, ANOVA).

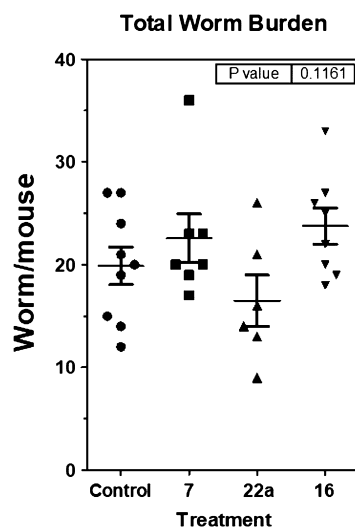


Figure 7. Schistosome recovery from infected mice, following administration of the indicated SmCA inhibitors (7, 16, and 22a) *vs* control. Each dot represents the worm burden from a single mouse and the lines indicate the means (\pm SEM) for each group.

CONCLUSIONS

Here, we report on the first crystallographic analysis of the schistosome tegumental enzyme SmCA complexed with CA inhibitors that preferentially block the activity of the parasite enzyme compared to human CA isoforms I and II. Information from these studies provides a foundation for understanding SARs between selenoureido and its isoster derivatives and SmCA showing different favorable/unfavorable contacts between the inhibitor tail moiety and the enzyme active site, leading to different inhibition profiles for this class of sulfonamides. Our results suggest a close correlation between the determined kinetic and X-ray crystallographic data and the selectivity profiles of selenoureido and its isosters. Although the three compounds tested here for their anti-schistosome impact were unable to kill worms in infected mice, nonetheless, such comparative crystallographic information as obtained in

this work should, in the longer term, help in the identification of novel, lead molecules that selectively inhibit SmCA and could become new, clinically useful, anti-schistosome therapeutics to impede vital parasite biochemistry and debilitate these important global pathogens.

EXPERIMENTAL SECTION

General. Anhydrous solvents and all reagents were purchased from Sigma-Aldrich, VWR, and TCI. All reactions involving air- or moisture-sensitive compounds were performed under a nitrogen atmosphere. Nuclear magnetic resonance (^1H NMR and ^{13}C NMR) spectra were recorded using a Bruker Advance III 400 MHz spectrometer in DMSO- d_6 or CDCl_3 . Chemical shifts are reported in parts per million (ppm) and the coupling constants (J) are expressed in Hertz (Hz). Splitting patterns are designated as follows: s, singlet; d, doublet; t, triplet; m, multiplet; brs, broad singlet; and dd, double of doubles. The assignment of exchangeable protons (NH) was confirmed by the addition of D_2O . Analytical thin-layer chromatography (TLC) was carried out on Merck silica gel F-254 plates. Flash chromatography purifications were performed with Merck silica gel 60 (230–400 mesh ASTM) as the stationary phase and ethyl acetate, *n*-hexane, acetonitrile, and methanol were used as eluents. The solvents used in MS measurements were acetone, acetonitrile (Chromasolv grade), purchased from Sigma-Aldrich (Milan, Italy), and Milli-Q water 18 M Ω , obtained from the Millipore's Simplicity system (Milan, Italy). The mass spectra were obtained using a Varian 1200L triple quadrupole system (Palo Alto, CA, USA) equipped with an electrospray source (ESI) operating on both positive and negative ions. Stock solutions of analytes were prepared in acetone at 1.0 mg mL $^{-1}$ and stored at 4 °C. Working solutions of each analyte were freshly prepared by diluting stock solutions with a mixture of Milli-Q H_2O /ACN 1/1 (v/v) up to a concentration of 1.0 μg mL $^{-1}$. The mass spectra of each analyte were acquired by introducing, *via* syringe pump at 10/L min $^{-1}$, the working solution. The raw data were collected and processed using Varian workstation, version 6.8, software. All compounds reported here are of >95% purity.

General Procedure for the Synthesis of Seleno, Thio, and Ureido Derivatives (5–19, 22a–b, and 23). The appropriate isoselenocyanate (1a–i), thiocyanate (20b, 21), or isocyanate (20a) (1 equiv) was dissolved in acetonitrile and treated with the corresponding benzenesulfonamide 2–4 (1 equiv). The mixture was stirred overnight at r.t. quenched with H_2O , and the readily formed precipitate was collected by filtration and dried in air to afford the titled selenourea 5–19, ureido 22a, and thioureido 22b and 23. The experimental data were in agreement with the reported data.^{29,31}

4-(2-(3-(4-Iodophenyl)thioureido)ethyl)benzenesulfonamide (23). Following the general procedure, the product was a white solid 23 with 71% yield. ^1H NMR (400 MHz, DMSO- d_6) δ (ppm): 9.65 (1H, br s), 7.90 (1H, br s), 7.81 (2H, d, J = 8.08 Hz), 7.66 (2H, d, J = 8.54 Hz), 7.48 (2H, d, J = 8.09 Hz), 7.35 (2H, br s), 7.23 (2H, d, J = 8.53 Hz), 3.76 (2H, m), 2.99 (2H, t, J = 7.14 Hz); ^{13}C NMR (100 MHz, DMSO- d_6) δ (ppm): 181.2, 144.4, 143.1, 140.0, 138.1, 130.1, 126.7, 126.0, 88.9, 45.8, 35.0; MS (ESI positive) m/z : 462 [M + H] $^+$.

Synthesis of Phenyl (4-Iodophenyl)carbamate (26). 4-Iodoaniline (1 equiv) and phenyl chloroformate (1 equiv) were added in acetone at 0 °C. Subsequently, K_2CO_3 (1.3 equiv) was added and the mixture was stirred for 30 min. The solvent was removed under a vacuum, water was added, and the precipitate was filtered off. The product was a light purple solid 26 with yield 90%. ^1H NMR (400 MHz, CDCl_3) δ (ppm): 7.26 (2H, d, J = 8.44 Hz), 7.37 (2H, apt, J = 7.72 Hz), 7.26–7.19 (3H, m), 7.15 (2H, d, J = 8.09 Hz), 6.89 (1H, br s); ^{13}C NMR (100 MHz, CDCl_3) δ (ppm): 151.7, 150.8, 138.4, 137.6, 138.1, 129.9, 126.2, 121.9, 121.0; MS (ESI positive) m/z : 340 [M + H] $^+$.

4-(2-(3-(4-Iodophenyl)ureido)ethyl)benzenesulfonamide (27). A mixture of (4-iodophenyl)carbamate (26) (1 equiv) and 4-(2-aminoethyl)benzenesulfonamide (4) (1 equiv) in acetonitrile was stirred at reflux overnight. Then, water was added, and the precipitate was filtered off. The product was a white solid 27 with yield 80%. ^1H

NMR (400 MHz, DMSO- d_6) δ (ppm): 8.63 (1H, br s), 7.80 (2H, d, J = 7.82 Hz), 7.56 (2H, d, J = 8.35 Hz), 7.46 (2H, d, J = 7.85 Hz), 7.33 (2H, br s), 7.28 (2H, d, J = 8.34 Hz), 6.22 (1H, br s), 3.41–3.40 (2H, m), 2.87 (2H, t, J = 6.61 Hz); ^{13}C NMR (100 MHz, DMSO- d_6) δ (ppm): 155.8, 144.6, 143.0, 141.3, 138.1, 130.0, 126.6, 120.8, 84.4, 41.1, 36.4; MS (ESI positive) m/z : 446 [M + H] $^+$.

Carbonic Anhydrase Inhibition. An applied photophysics stopped-flow instrument was used to assay the CA-catalyzed CO_2 -hydration activity.³⁰ Phenol red (at a concentration of 0.2 mM) was used as an indicator, working at an absorbance maximum of 557 nm, with 20 mM HEPES (pH 7.4) as a buffer and 20 mM Na_2SO_4 (to maintain constant ionic strength), following the initial rates of the CA-catalyzed CO_2 -hydration reaction for a period of 10–100 s. The CO_2 concentrations ranged from 1.7 to 17 mM for the determination of the kinetic parameters and inhibition constants.¹⁸ The enzyme concentrations ranged between 5 and 12 nM. For each inhibitor, at least six traces of the initial 5–10% of the reaction were used to determine the initial velocity. The uncatalyzed rates were determined in the same manner and subtracted from the total observed rates. Stock solutions of the inhibitor (0.1 mM) were prepared with distilled–deionized water and dilutions up to 0.01 nM were carried out thereafter with the assay buffer. The inhibitor and enzyme solutions were pre-incubated together for 15 min at room temperature prior to the assay, to allow for the formation of the E–I complex. The inhibition constants were obtained by non-linear least squares methods using PRISM 3 and the Cheng–Prusoff equation as reported earlier and represent the mean from at least three different determinations. All CA isoforms were recombinant proteins obtained in house, as reported earlier.^{16,34–36}

Parasites and Mice. The Puerto Rican strain of *S. mansoni* was used. Adult male and female parasites were recovered by perfusion from female 6–8 week old Swiss Webster mice that were infected with ~90 cercariae, 9 weeks previously.³⁷ All protocols involving animals were approved by the Institutional Animal Care and Use Committees (IACUC) of Tufts University. Pilot experiments, as described,³⁸ determined that the maximum tolerable dose for the mice of compounds 7 and 16 was 100 mg/kg and for 22a was 50 mg/kg. At day 42, 44, and 46 post infection, groups of mice were administered each compound intraperitoneally at this dosage. Control mice were treated with carrier (20% DMSO) alone. Two weeks after the final treatment, all mice were perfused and worm numbers recovered per animal were calculated.

Crystallization and X-ray Data Collection. The SmCA enzyme, purified in the recombinant form, as described previously,¹⁶ was crystallized at 296 K using the sitting-drop vapor-diffusion method in 96-well plates (CrystalQuick, Greiner Bio-One, Germany). Drops were prepared using 1 μL protein solution mixed with 1 μL reservoir solution and were equilibrated against 100 μL precipitant solution. The concentration of the protein was 10 mg mL $^{-1}$ in 50 mM Tris pH 8.3. Initial crystallization conditions were found using the JCSG-plus screen (Molecular Dimensions) and were optimized. Crystals of the native protein were prepared using a solution of 0.2 M zinc acetate dihydrate, 0.1 M imidazole pH 8.0, and 20% w/v PEG 3000, and they belonged to the primitive tetragonal space group $P4_12_12$. Crystals of the complex with compounds 18 and 8 were prepared using a solution of 20% PEG 3350, 0.2 M di-ammonium hydrogen citrate. Crystals of the complex with 22a–b, 23, and 27 were obtained using 20% PEG 6000 and 0.1 M citrate (pH 5.0). The crystals belonged to the primitive trigonal space group $P3_121$. The complexes were prepared by soaking the SmCA native crystals in the mother liquor solution containing the inhibitors at a concentration of 10 mM for two days. Crystals of hCA II were obtained using the hanging-drop vapor-diffusion method using a 24-well Linbro plate. 2 μL of 10 mg/mL solution of hCA II in 20 mM Tris–HCl (pH 8.0) was mixed with 2 μL of a solution of 1.5 M sodium citrate and 0.1 M Tris pH (8.0) and was equilibrated against the same solution at 296 K. The complexes were prepared by soaking the hCA II native crystals in the mother liquor solution containing the inhibitors at a concentration of 10 mM for two days. All crystals were flash-frozen at 100 K using a solution obtained by adding 15% (v/v) glycerol to the mother liquor solution

as a cryoprotectant. The data on crystals of the complexes were collected using synchrotron radiation at the XRD2 beamline at the Elettra Synchrotron (Trieste, Italy) with a wavelength of 1.000 Å and a DECTRIS PILATUS 6M detector. The data on a tetragonal crystal of the native SmCA were collected using synchrotron radiation at the ID-30B beamline at ESRF (Grenoble, France) with a wavelength of 0.827 Å and a PILATUS3 6M Dectris CCD detector. The data were integrated and scaled using the program XDS.³⁹ Data processing statistics are shown in [Supporting Information](#).

Structure Determination. The crystal structure of hCA II (PDB accession code: 4FIK) and SmCA (PDB accession code: 6QQM) without solvent molecules and other heteroatoms was used to obtain initial phases using RefmacS.⁴⁰ 5% of the unique reflections was selected randomly and excluded from the refinement data set for the purpose of Rfree calculations. The initial |Fo – Fcl difference electron density maps unambiguously showed the inhibitor molecules. The inhibitor was introduced in the model with 1.0 or 0.7 occupancy. Refinements proceeded using normal protocols of positional, isotropic atomic displacement parameters alternating with manual building of the models using COOT.⁴¹ The quality of the final models was assessed with COOT and RAMPAGE.⁴² The crystal parameters and refinement data are summarized in [Supporting Information](#). Atomic coordinates were deposited in the Protein Data Bank (PDB accession code: 7BG5; 7BFA; 7BHH; 7NWY; 7BM4; 7NEX; 7NG1; 7O48; 7OAI; and 7O2S). The graphical representations were generated with Chimera.⁴³

■ ASSOCIATED CONTENT

SI Supporting Information

The Supporting Information is available free of charge at <https://pubs.acs.org/doi/10.1021/acs.jmedchem.1c00840>.

Molecular formula string file (CSV)

¹H and ¹³C NMR spectra of compounds 23, 26, and 27; summary of data collection and atomic model refinement statistics for hCA II and SmCA; electron density of inhibitors bound to zinc; and compounds 27, 23 and 18 inside the active site of SmCA (PDF)

■ AUTHOR INFORMATION

Corresponding Authors

Andrea Angeli – *NEUROFARBA Department, Sezione di Scienze Farmaceutiche, University of Florence, 50019 Florence, Italy; Centre of Advanced Research in Bionanoconjugates and Biopolymers Department, “Petru Poni” Institute of Macromolecular Chemistry, 707410 Iasi, Romania; orcid.org/0000-0002-1470-7192; Phone: +39 055 457 3666; Email: andrea.angeli@unifi.it*

Marta Ferraroni – *Dipartimento di Chimica “Ugo Schiff”, University of Florence, 50019 Florence, Italy; orcid.org/0000-0001-7258-738X; Phone: +39 055 457 3342; Email: marta.ferraroni@unifi.it*

Authors

Akram A. Da'dara – *Department of Infectious Disease and Global Health, Cummings School of Veterinary Medicine, Tufts University, North Grafton, Massachusetts 01536, United States*

Silvia Selleri – *NEUROFARBA Department, Sezione di Scienze Farmaceutiche, University of Florence, 50019 Florence, Italy*

Mariana Pinteala – *Centre of Advanced Research in Bionanoconjugates and Biopolymers Department, “Petru Poni” Institute of Macromolecular Chemistry, 707410 Iasi, Romania*

Fabrizio Carta – *NEUROFARBA Department, Sezione di Scienze Farmaceutiche, University of Florence, 50019 Florence, Italy; orcid.org/0000-0002-1141-6146*

Patrick J. Skelly – *Department of Infectious Disease and Global Health, Cummings School of Veterinary Medicine, Tufts University, North Grafton, Massachusetts 01536, United States*

Claudiu T. Supuran – *NEUROFARBA Department, Sezione di Scienze Farmaceutiche, University of Florence, 50019 Florence, Italy; orcid.org/0000-0003-4262-0323*

Complete contact information is available at: <https://pubs.acs.org/doi/10.1021/acs.jmedchem.1c00840>

Author Contributions

The article was written through contributions of all authors. All authors have given approval to the final version of the article.

Funding

This work was supported by a grant of the Romanian Ministry of Research and Innovation, CNCS–UEFISCDI, project number PN-III-P4-ID-PCCF-2016–0050, within PNCDI II. This work was also financed by the Italian Ministry of University and Research, project FIS2019_04819 BacCAD (CTS). This work was additionally supported by grant AI111011 from the National Institutes of Health–National Institute of Allergy and Infectious Diseases (NIH–NIAID). Schistosome-infected snails were provided by the Biomedical Research Institute through NIH–NIAID contract HHSN272201000009.

Notes

The authors declare no competing financial interest.

■ ABBREVIATIONS

CA, carbonic anhydrase; CAI, carbonic anhydrase inhibitors; TLC, thin layer chromatography

■ REFERENCES

- (1) King, C. H.; Dickman, K.; Tisch, D. J. Reassessment of the cost of chronic helminthic infection: a meta-analysis of disability-related outcomes in endemic schistosomiasis. *Lancet* **2005**, *365*, 1561–1569.
- (2) Steinmann, P.; Keiser, J.; Bos, R.; Tanner, M.; Utzinger, J. Schistosomiasis and water resources development: systematic review, meta-analysis, and estimates of people at risk. *Lancet Infect. Dis.* **2006**, *6*, 411–425.
- (3) Utzinger, J.; Raso, G.; Brooker, S.; De Savigny, D.; Tanner, M.; Ørnberg, N.; Singer, B. H.; N'goran, E. K. Schistosomiasis and neglected tropical diseases: towards integrated and sustainable control and a word of caution. *Parasitology* **2009**, *136*, 1859–1874.
- (4) Hotez, P. J.; Alvarado, M.; Basáñez, M.-G.; Bolliger, I.; Bourne, R.; Boussinesq, M.; Brooker, S. J.; Brown, A. S.; Buckle, G.; Budke, C. M.; Carabin, H.; Coffeng, L. E.; Fèvre, E. M.; Fürst, T.; Halasa, Y. A.; Jasrasaria, R.; Johns, N. E.; Keiser, J.; King, C. H.; Lozano, R.; Murdoch, M. E.; O'Hanlon, S.; Pion, S. D. S.; Pullan, R. L.; Ramaiah, K. D.; Roberts, T.; Shepard, D. S.; Smith, J. L.; Stolk, W. A.; Undurraga, E. A.; Utzinger, J.; Wang, M.; Murray, C. J. L.; Naghavi, M. The global burden of disease Study 2010: interpretation and implications for the neglected tropical diseases. *PLoS Neglected Trop. Dis.* **2014**, *8*, No. e2865.
- (5) Rollinson, D.; Knopp, S.; Levitz, S.; Stothard, J. R.; Tchuem Tchuenté, L.-A.; Garba, A.; Mohammed, K. A.; Schur, N.; Person, B.; Colley, D. G.; Utzinger, J. Time to set the agenda for schistosomiasis elimination. *Acta Trop.* **2013**, *128*, 423–440.
- (6) van der Werf, M. J.; de Vlas, S. J.; Brooker, S.; Looman, C. W. N.; Nagelkerke, N. J. D.; Habbema, J. D. F.; Engels, D. Quantification

of clinical morbidity associated with schistosome infection in sub-Saharan Africa. *Acta Trop.* **2003**, *86*, 125–139.

(7) Colley, D. G.; Bustinduy, A. L.; Secor, W. E.; King, C. H. Human schistosomiasis. *Lancet* **2014**, *383*, 2253–2264.

(8) Mo, A. X.; Gordon, L.; Hall, B. F.; Walson, J. L.; Agosti, J. M. Schistosomiasis elimination strategies and potential role of a vaccine in achieving global health goals. *Am. J. Trop. Med. Hyg.* **2014**, *90*, 54–60.

(9) Mo, A. X.; Colley, D. G. Workshop report: schistosomiasis vaccine clinical development and product characteristics. *Vaccine* **2016**, *34*, 995–1001.

(10) Aruleba, R. T.; Adekiya, T. A.; Oyinloye, B. E.; Masamba, P.; Mbatha, L. S.; Pretorius, A.; Kappo, A. P. PZQ therapy: how close are we in the development of effective alternative anti-schistosomal drugs? *Infect. Disord.-Drug Targets* **2019**, *19*, 337–349.

(11) Silva, I. M. d.; Thiengo, R.; Conceição, M. J.; Rey, L.; Lenzi, H. L.; Pereira Filho, E.; Ribeiro, P. C. Therapeutic failure of praziquantel in the treatment of schistosoma haematobium infection in brazilians returning from africa. *Mem. Inst. Oswaldo Cruz* **2005**, *100*, 445–449.

(12) Melman, S. D.; Steinauer, M. L.; Cunningham, C.; Kubatko, L. S.; Mwangi, I. N.; Wynn, N. B.; Mutuku, M. W.; Karanja, D. M. S.; Colley, D. G.; Black, C. L.; Secor, W. E.; Mkoji, G. M.; Loker, E. S. Reduced susceptibility to praziquantel among naturally occurring kenyan isolates of schistosoma mansoni. *PLoS Neglected Trop. Dis.* **2009**, *3*, No. e504.

(13) Pica-Mattocchia, L.; Doenhoff, M. J.; Valle, C.; Basso, A.; Troiani, A.-R.; Liberti, P.; Festucci, A.; Guidi, A.; Cioli, D. Genetic analysis of decreased praziquantel sensitivity in a laboratory strain of schistosoma mansoni. *Acta Trop.* **2009**, *111*, 82–85.

(14) Braschi, S.; Wilson, R. A. Proteins exposed at the adult schistosome surface revealed by biotinylation. *Mol. Cell. Proteomics* **2006**, *5*, 347–356.

(15) Castro-Borges, W.; Dowle, A.; Curwen, R. S.; Thomas-Oates, J.; Wilson, R. A. Enzymatic shaving of the tegument surface of live schistosomes for proteomic analysis: a rational approach to select vaccine candidates. *PLoS Neglected Trop. Dis.* **2011**, *5*, No. e993.

(16) Da'dara, A. A.; Angeli, A.; Ferraroni, M.; Supuran, C. T.; Skelly, P. J. Crystal structure and chemical inhibition of essential schistosome host-interactive virulence factor carbonic anhydrase SmCA. *Commun. Biol.* **2019**, *2*, 333.

(17) Angeli, A.; Pinteala, M.; Maier, S. S.; Simionescu, B. C.; Da'dara, A. A.; Skelly, P. J.; Supuran, C. T. Sulfonamide inhibition studies of an α -Carbonic anhydrase from schistosoma mansoni, a platyhelminth parasite responsible for schistosomiasis. *Int. J. Mol. Sci.* **2020**, *21*, 1842.

(18) Supuran, C. T. Carbonic anhydrases: novel therapeutic applications for inhibitors and activators. *Nat. Rev. Drug Discov.* **2008**, *7*, 168–181.

(19) Supuran, C. T. Structure and function of carbonic anhydrases. *Biochem. J.* **2016**, *473*, 2023–2032.

(20) Supuran, C.; Capasso, C. An overview of the bacterial carbonic anhydrases. *Metabolites* **2017**, *7*, 56.

(21) Mishra, C. B.; Tiwari, M.; Supuran, C. T. Progress in the development of human carbonic anhydrase inhibitors and their pharmacological applications: Where are we today? *Med. Res. Rev.* **2020**, *40*, 2485–2565.

(22) Mansoldo, F. R. P.; Carta, F.; Angeli, A.; Cardoso, V. D. S.; Supuran, C. T.; Vermelho, A. B. Chagas disease: perspectives on the past and present and challenges in drug discovery. *Molecules* **2020**, *25*, 5483.

(23) Angeli, A.; Etxebeste-Mitxelorena, M.; Sanmartín, C.; Espuelas, S.; Moreno, E.; Azqueta, A.; Parkkila, S.; Carta, F.; Supuran, C. T. Tellurides bearing sulfonamides as novel inhibitors of leishmanial carbonic anhydrase with potent antileishmanial Activity. *J. Med. Chem.* **2020**, *63*, 4306–4314.

(24) Al-Tamimi, A.-M. S.; Etxebeste-Mitxelorena, M.; Sanmartín, C.; Jiménez-Ruiz, A.; Syrjänen, L.; Parkkila, S.; Selleri, S.; Carta, F.; Angeli, A.; Supuran, C. T. Discovery of new organoselenium

compounds as antileishmanial agents. *Bioorg. Chem.* **2019**, *86*, 339–345.

(25) D'Ambrosio, K.; Supuran, C. T.; De Simone, G. Are carbonic anhydrases suitable targets to fight protozoan parasitic diseases? *Curr. Med. Chem.* **2019**, *25*, 5266–5278.

(26) Lou, Y.; McDonald, P. C.; Oloumi, A.; Chia, S.; Ostlund, C.; Ahmadi, A.; Kyle, A.; Auf dem Keller, U.; Leung, S.; Huntsman, D.; Clarke, B.; Sutherland, B. W.; Waterhouse, D.; Bally, M.; Roskelley, C.; Overall, C. M.; Minchinton, A.; Pacchiano, F.; Carta, F.; Scozzafava, A.; Touisni, N.; Winum, J.-Y.; Supuran, C. T.; Dedhar, S. Targeting tumor hypoxia: suppression of breast tumor growth and metastasis by novel carbonic anhydrase IX inhibitors. *Cancer Res.* **2011**, *71*, 3364–3376.

(27) Supuran, C. Carbonic anhydrases—an overview. *Curr. Pharm. Des.* **2008**, *14*, 603–614.

(28) Supuran, C. T. Structure-based drug discovery of carbonic anhydrase inhibitors. *J. Enzyme Inhib. Med. Chem.* **2012**, *27*, 759–772.

(29) Angeli, A.; Tanini, D.; Peat, T. S.; Di Cesare Mannelli, L.; Bartolucci, G.; Capperucci, A.; Ghelardini, C.; Supuran, C. T.; Carta, F. Discovery of new selenoureido analogues of 4-(4-Fluorophenylureido)benzenesulfonamide as carbonic anhydrase inhibitors. *ACS Med. Chem. Lett.* **2017**, *8*, 963–968.

(30) Khalifah, R. G. The carbon dioxide hydration activity of carbonic anhydrase. I. Stop flow kinetic studies on the native human isoenzymes B and C. *J. Biol. Chem.* **1971**, *246*, 2561–2573.

(31) Pacchiano, F.; Carta, F.; McDonald, P. C.; Lou, Y.; Vullo, D.; Scozzafava, A.; Dedhar, S.; Supuran, C. T. Ureido-substituted benzenesulfonamides potently inhibit carbonic anhydrase IX and show antimetastatic activity in a model of breast cancer metastasis. *J. Med. Chem.* **2011**, *54*, 1896–1902.

(32) Pacchiano, F.; Aggarwal, M.; Avvaru, B. S.; Robbins, A. H.; Scozzafava, A.; McKenna, R.; Supuran, C. T. Selective hydrophobic pocket binding observed within the carbonic anhydrase II active site accommodate different 4-substituted-ureido-benzenesulfonamides and correlate to inhibitor potency. *Chem. Commun.* **2010**, *46*, 8371–8373.

(33) Mboge, M. Y.; Mahon, B. P.; Lamas, N.; Socorro, L.; Carta, F.; Supuran, C. T.; Frost, S. C.; McKenna, R. Structure activity study of carbonic anhydrase IX: Selective inhibition with ureido-substituted benzenesulfonamides. *Eur. J. Med. Chem.* **2017**, *132*, 184–191.

(34) Mocan, A.; Carradori, S.; Locatelli, M.; Secci, D.; Cesa, S.; Mollica, A.; Riga, S.; Angeli, A.; Supuran, C. T.; Celia, C.; Di Marzio, L. Bioactive isoflavones from Pueraria lobata root and starch: Different extraction techniques and carbonic anhydrase inhibition. *Food Chem. Toxicol.* **2018**, *112*, 441–447.

(35) De Vita, D.; Angeli, A.; Pandolfi, F.; Bortolami, M.; Costi, R.; Di Santo, R.; Suffredini, E.; Ceruso, M.; Del Prete, S.; Capasso, C.; Scipione, L.; Supuran, C. T. Inhibition of the α -carbonic anhydrase from Vibrio cholerae with amides and sulfonamides incorporating imidazole moieties. *J. Enzyme Inhib. Med. Chem.* **2017**, *32*, 798–804.

(36) Angeli, A.; Carta, F.; Bartolucci, G.; Supuran, C. T. Synthesis of novel acyl selenoureido benzenesulfonamides as carbonic anhydrase I, II, VII and IX inhibitors. *Bioorg. Med. Chem.* **2017**, *25*, 3567–3573.

(37) Tucker, M. S.; Karunaratne, L. B.; Lewis, F. A.; Freitas, T. C.; Liang, Y. S. Schistosomiasis. *Curr. Protoc. Im.* **2013**, *103*, 11.

(38) Ramirez, B.; Bickle, Q.; Yousif, F.; Fakorede, F.; Mouries, M.-A.; Nwaka, S. Schistosomes: challenges in compound screening. *Expert Opin. Drug Discov.* **2007**, *2*, S53–S61.

(39) Leslie, A. G. W.; Powell, H. R. Processing diffraction data with mosflm. In *Evolving Methods for Macromolecular Crystallography*; Read, R. J., Sussman, J. L., Eds.; NATO Science series; Springer: Dordrecht, 2007; Vol. 245, pp 41–51.

(40) Murshudov, G. N.; Vagin, A. A.; Dodson, E. J. Refinement of macromolecular structures by the maximum-likelihood method. *Acta Crystallogr., Sect. D: Biol. Crystallogr.* **1997**, *53*, 240–255.

(41) Emsley, P.; Lohkamp, B.; Scott, W. G.; Cowtan, K. Features and development of Coot. *Acta Crystallogr., Sect. D: Biol. Crystallogr.* **2010**, *66*, 486–501.

(42) Lovell, S. C.; Davis, I. W.; Arendall, W. B., III; de Bakker, P. I. W.; Word, J. M.; Prisant, M. G.; Richardson, J. S.; Richardson, D. C. Structure validation by $C\alpha$ geometry: ϕ , ψ and $C\beta$ deviation. *Proteins* **2003**, *50*, 437–450.

(43) Pettersen, E. F.; Goddard, T. D.; Huang, C. C.; Couch, G. S.; Greenblatt, D. M.; Meng, E. C.; Ferrin, T. E. UCSF Chimera—a visualization system for exploratory research and analysis. *J. Comput. Chem.* **2004**, *25*, 1605–1612.